Michigan State University

National Superconducting Cyclotron Laboratory

EFFICIENCY OF A BaF_2 SCINTILLATOR DETECTOR FOR 15 - 150 MeV NEUTRONS

R.A. KRYGER, A. AZHARI, E. RAMAKRISHNAN, M. THOENNESSEN, and S. YOKOYAMA

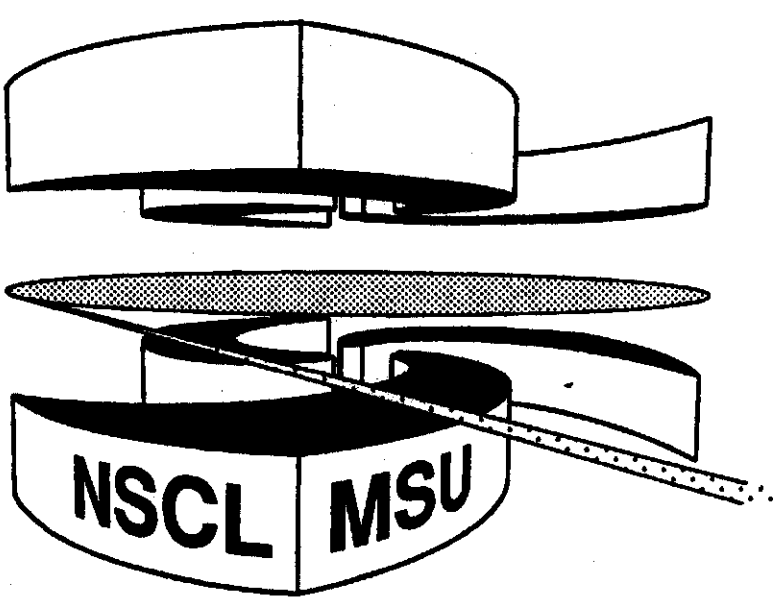

MSUCL-927

APRIL 1994

MSUCL-927

Efficiency of a BaF_2 Scintillator Detector for 15 - 150 MeV Neutrons'

R. A. Kryger[1], A. Azhari[1,2], E. Ramakrishnan[1,2], M. Thoennessen[1,2], and S. Yokoyama[1,2]

'National Superconducting Cyclotron Laboratory, Michigan State University, East Lansing, MI 48824-1321

*Department of physics and Astronomy, Michigan State University, East Lansing, MI 48824

(April 9, 1994)

Abstract

The neutron detection efficiency of a BaF_2 scintillator detector was measured relative to a NE213 detector for neutron energies between 15 and 150 MeV. The efficiency for the BaF_2 detector is found to be higher than a comparable NE213 detector for neutrons above 70 MeV.

Typeset using REVTEX

INTRODUCTION

BaF_2 scintillator detectors are now in common use for the measurement of γ-rays over a wide energy range because of the relatively high detection efficiency and the fast response which allows subnanosecond timing [1,2]. The BaF_2 scintillation light consists primarily of two components with decay times of $\tau_1 \approx 600$ ps and $\tau_2 \approx 620$ ns [2], and the ratio of the intensities associated with each of these components is sensitive to the incident radiation type [3]. One particularly interesting feature of BaF_2 detectors is that it is possible to distinguish neutron-induced interactions from γ-ray interactions for relatively high energy neutrons ($E_n > 10$ MeV) using pulse shape discrimination (PSD) techniques [4,6]. This separation is thought to result from neutron reactions in the BaF_2 which emit light charged particles (p,d,^{4}He,...) in contrast to γ-rays which interact primarily through electrons [4]. The n/γ pulse shape discrimination coupled with the good timing properties makes BaF_2 a potentially attractive neutron detector. Unfortunately, there is very little information currently available regarding the neutron efficiency of BaF_2, in contrast to the situation with standard organic scintillators such as NE213 where computer codes are commonly available to calculate detector efficiencies over a wide range of neutron energies [5]. In fact, only two BaF_2 neutron efficiency measurements have been reported for neutron energies above 10 MeV [4,6]. Matulewicz, *et al.* [4] measured the BaF_2 neutron efficiency for neutron energies up to 22 MeV, but they did not employ neutron/γ pulse-shape discrimination. In the second paper, Kubota, *et al.* [6] reported the neutron efficiency of a BaF_2 detector for neutron energies between 15 and 45 MeV after imposing a PSD cut on neutron events. The BaF_2 detector efficiency was found to increase with neutron energy while the efficiency of a comparable NE213 detector decreased so that near 45 MeV the neutron efficiencies of the two scintillator detectors were similar. In this paper we present the results of an extended measurement to determine the BaF_2 efficiency for neutrons with energies up to 150 MeV. Furthermore, we present detector response data as a function of light output for neutrons at two different energies which will be useful to compare with any future calculations of BaF_2

detector response to neutrons.

EXPERIMENTAL DETAILS

The BaF_2 detector in our measurement consisted of a 25 cm long hexagonal BaF_2 crystal with a 5.9 cm edge-to-edge front face coupled to a fast phototube. The phototube had a quartz entrance window to minimize the attenuation of the ultraviolet BaF_2 scintillation light. A 7.6 cm long cylindrical NE213 liquid-scintillator cell with 12.7 cm diameter coupled to a standard phototube was used as a reference detector. Neutrons over a broad energy range were produced by using a pulsed 70 MeV/A ^{14}N beam from the National Superconducting Cyclotron Laboratory K1200 cyclotron incident on a 1.3 cm thick brass beam stop. The time period between beam bursts was 57.8 ns. The two neutron detectors were placed at 23° with respect to the beam axis, slightly above and below the horizontal plane. A thin plastic scintillator detector was placed in front of the two detectors to veto incident charged particles. Data was taken at two detector distances in order to cover a broad range of neutron energies. The detector centers were placed at a nominal distance of 5.3 m from the target (5.36 m for the BaF_2 detector and 5.29 m for the NE213 detector) in the first run and at a nominal distance of 2.4 m from the target (2.43 m for the BaF_2 detector and 2.36 m for the NE213 detector) for the second run. During each run events in both detectors, consisting of the time-of-flight (TOF), light output, and pulse-shape signals, were recorded independently. Signals in the plastic veto detector were also recorded when present. The TOF signal was measured relative to the cyclotron RF, and the absolute neutron TOF was determined relative to the peak in the time spectrum associated with γ-rays emitted from the target. For the purpose of this TOF calibration, the target γ-rays, which consist primarily of low-energy photons, were assumed to interact in the center of the low-Z NE213 detector. However, for the BaF_2 detector, we assumed the average interaction occurred at a depth of 2.3 cm from the front face of the detector, corresponding to the measured absorption length for 511 keV photons in BaF_2 [7]. Neutrons were assumed to interact in the center of both de-

tectors. The full-width at half-maximum (FWHM) of the γ-peak, yielding a measure of the timing resolution, was 1.3 ns for the BaF_2 detector and 0.9 ns for the NE213 detector. The total BaF_2 light output was determined by integrating the phototube anode output pulse using a charge-to-digital converter (QDC) with a 1.5 μs wide gate. The NE213 light output was obtained similarly using an integration time of 400 ns. The light output was calibrated in electron equivalent MeV (MeV-ee) using γ-ray source measurements in both detectors and the cosmic peak in the BaF_2 detector [8]. The PSD signal for the BaF_2 detector was obtained by integrating the first $\sim$ 30 ns of the phototube anode signal, corresponding to the fast light peak [6], using a QDC. The NE213 detector PSD signal was determined by integrating the tail of the anode signal by activating the QDC gate $\sim$ 35 ns after the start of the anode output pulse [9]. Neutron/γ-ray discrimination in both detectors was achieved offline using two-dimensional conditions defined on histograms of the PSD signal versus the total light output signal.

ANALYSIS AND RESULTS

Figures 1 and 2 show the TOF spectra obtained for both detectors at the near (2.4 m) and the far (5.3 m) positions after application of pulse-shape cuts for neutrons and after vetoing charged-particle induced events using the veto scintillator. The NE213 detector has a software-imposed lower-threshold on the light output corresponding to 3.9 MeV-ee in order to remove the overlap of long TOF (low-energy) neutrons from the previous beam burst into the region of interest in the 2.4 m data. This overlapping is still clearly present in the 5.3 m data for both of the detectors. The light threshold on the BaF_2 detector data, determined by the PSD gate on the neutrons, corresponds to 7.0 MeV-ee. The estimated TOF background in the 5.3 m data associated with the neutrons from the previous beam burst is shown in Figure 2 by the dotted lines. This background was obtained by transforming the data for each detector taken at the near distance to the appropriate far distance, shifting the time by 57.8 ns (the time between cyclotron beam bursts), and normalizing the resulting spectrum

to the data in the region of the tail of the previous beam burst. Once the TOF background was subtracted, the corrected time spectra were normalized by the detector solid angle, transformed to a distance of 5.30 m, and binned into 1 ns wide bins corresponding to the approximate time resolution. The time spectra for the near distance run were treated in a similar fashion although no background subtraction was necessary.

The BaF_2 detector efficiency was computed as a function of TOF according to the relationship

$$\epsilon_{BaF}(t) = \frac{\left(\frac{dY_{BaF}(t)}{dt\Delta\Omega_{BaF}}\right)}{\left(\frac{dY_r(t)}{dt\Delta\Omega_r}\right)\left(\frac{1}{\epsilon_r(t)}\right)} \tag{1}$$

where $dY_{BaF}(t)/dt\Delta\Omega_{BaF}$ and $dY_r(t)/dt\Delta\Omega_r$ are the time spectra for the BaF_2 and NE213 reference detectors transformed to the same neutron flight path distance, respectively, and $\epsilon_r(t)$ is the absolute neutron detection efficiency of the NE213 detector for neutrons with energy corresponding to time-of-flight t. The NE213 detector efficiency $\epsilon_r(t)$ was calculated using the Monte Carlo program of Cecil *et al.* [10] which was written for modeling hydrocarbon scintillator response to neutrons. The calculation incorporated the NE213 scintillator geometry and the 3.9 MeV-ee light threshold. Figure 3 shows the calculated NE213 efficiency which we used to evaluate Eq. 1 as a function of neutron energy between 10 and 150 MeV. The BaF_2 efficiency determined from this analysis for both the near (squares) and far (circles) detector positions is shown in Figure 4 as a function of neutron energy. The error bars reflect the statistical uncertainties in the TOF data and a $\pm 5\%$ uncertainty assumed for the calculated NE213 detector efficiency. The effect of the 1 ns time bins transformed to neutron energy can be seen in the spacing of the data along the x-axis. The solid and dashed lines in Figure 4 show calculated efficiency functions for a cylindrical NE213 scintillator detector with the same length and volume as the hexagonal BaF_2 detector used in the present measurement. The two lines correspond to a light threshold of 7.0 MeV-ee (solid) and 0.5 MeV-ee (dashed) to illustrate the effect of the light threshold. Since the PSD between neutrons and photons in NE213 can typically be achieved well below a 7.0 MeV-ee light

threshold, the second calculation with a 0.5 MeV-ee threshold is a more practical efficiency curve to compare with the BaF_2 results. The BaF_2 neutron efficiency is seen to drop substantially below 50 MeV. This effect results primarily from the pulse shape discrimination requirement and the related 7.0 MeV-ee light threshold. Matulewicz, *et al.* [4] found that in the absence of the neutron PSD requirement, the BaF_2 neutron detection efficiency was approximately constant between 10 and 22 MeV with a 1.0 MeV-ee light threshold. Above 70 MeV neutron energy, the BaF_2 efficiency is found to surpass that of a comparable NE213 detector. Furthermore, the BaF_2 efficiency continues to increase with neutron energy while the NE213 efficiency is slowly decreasing.

Finally, the solid histograms in Figure 5 show the BaF_2 scintillator response as a function of light output for 50 and 75 MeV neutrons above the PSD threshold. For comparison, the calculated NE213 response for the same volume NE213 detector is shown by the dotted histograms, normalized by the total light output above 7.0 MeV-ee. The response function for the BaF_2 shows no evidence for a full-energy peak (weakly seen in the NE213 calculations) indicating that the energy resolution of the light output would be quite poor.

In summary, we have measured the neutron detection efficiency of a BaF_2 scintillator detector relative to a NE213 reference detector under the condition that neutrons are identified by pulse-shape discrimination techniques. Between 15 and 50 MeV, we find qualitative agreement with the previous results of Kubota, *et al.* [6] who showed that the BaF_2 neutron efficiency is increasing in this energy range. Furthermore we have extended the measurements up to 150 MeV and find that the BaF_2 efficiency surpasses that of a comparably sized NE213 detector for neutrons above $\sim$ 70 MeV. This high neutron detection efficiency, coupled with the pulse-shape discrimination and fast-timing features of BaF_2, indicate that BaF_2 can make a very suitable detector for high energy neutrons.

REFERENCES

* To be published in NIM A.

[1] R. Novotny, R. Riess, R. Hingmann, H. Ströher, R.D. Fisher, G. Koch, W. Kühn, V. Metag, R. Mühlhans, U. Kneissl, W. Wilke, B. Haas, J.P. Vivien, R. Beck, B. Schoch, and Y. Schutz, Nucl. Instrum. Meth. **A262** (1987) 340.

[2] M. Laval, M. Moszynski, R. Allemand, E. Cormoreche, P. Guinet, R. Odru, and J. Vacher, Nucl. Instrum. Meth. **206** (1983) 169.

[3] E. Dafni, Nucl. Instrum. Meth. **A254** (1987) 54.

[4] T. Matulewicz, E. Grosse, H. Emling, H. Grein, R. Kulessa, F.M. Baumann, G. Domogala, and H. Freiesleben, Nucl. Instrum. Meth. **A274** (1989) 501.

[5] See for example P. Desesquelles, A.J. Cole, A. Dauchy, A. Giorni, D. Heuer, A. Lleres, C. Morand, J. Saint-Martin, P. Stassi, J.B. Viano, B. Chambon, B. Cheynis, D. Drain, and C. Pastor, Nucl. Instrum. Meth. **A307** (1991) 366, Y. Uwamino, K. Shin, M. Fujii, and T. Nakamura, Nucl. Instrum. Meth. **204** (1982) 179, and R.A. Cecil, B.D. Anderson, and R. Madey, Nucl. Instrum. Meth. **161** (1979) 439, and references therein.

[6] S. Kubota, T. Motobayashi, M. Ogiwara, H. Murakami, Y. Ando, J. Ruan(gen), S. Shirato, and T. Murakami, Nucl. Instrum. Meth. **A285** (1989) 436.

[7] D.F. Anderson, IEEE Transactions on Nuclear Science, Vol. **NS-36** (1989) 137.

[8] L.G. Sobotka, L. Gallamore, A. Chbihi, D.G. Sarantites, D.W. Stacener, W. Bauer, D.R. Bowman, N. Carlin, R.T. DeSouza, C.K. Gelbke, W.G. Gong, S. Hannuschke, Y.K. Kim, W.G. Lynch, R. Ronningen, M.B. Tsang, F. Zhu, J.R. Beene, M.L. Halbert, and M. Thoennessen, Phys. Rev. **C44** (1991) R2257.

[9] J. Heltsky, L. Brandon, A. Galonsky, L. Heilbronn, B.A. Remington, S. Langer, A. Vander Molen, and J. Yurkon, Nucl. Instrum. Meth. **A263** (1988) 441.

[10] R.A. Cecil, B.D. Anderson, and R. Madey, Nucl. Instrum. Meth. **161** (1979) 439.

FIGURES

FIG. 1. Neutron time-of-flight spectra for the BaF_2 detector and the NE213 reference detector obtained at the 2.4 m detector positions.

FIG. 2. Neutron time-of-flight spectra for the BaF_2 detector and the NE213 reference detector obtained at the 5.3 m detector positions. The dotted lines show the TOF background due to low energy neutrons from the previous beam burst as estimated from the 2.4 m data.

FIG. 3. The calculated neutron detection efficiency for the NE213 reference detector as a function of neutron energy.

FIG. 4. The absolute neutron detection efficiency of the BaF_2 detector as a function of neutron energy for the 2.4 m data (squares) and the 5.3 m data (circles). The solid and dashed lines correspond to calculated efficiencies for a cylindrical NE213 detector of the same length and volume as the hexagonal BaF_2 detector with light thresholds of 7.0 and 0.5 MeV-ee, respectively.

FIG. 5. The BaF_2 detector response as a function of light output to 50 and 75 MeV neutrons (solid histogram). The dotted histograms show the calculated response for the same energy neutrons in a cylindrical NE213 detector with the same length and volume as the hexagonal BaF_2 detector, normalized to the total light output above 7.0 MeV-ee.

Figure 1

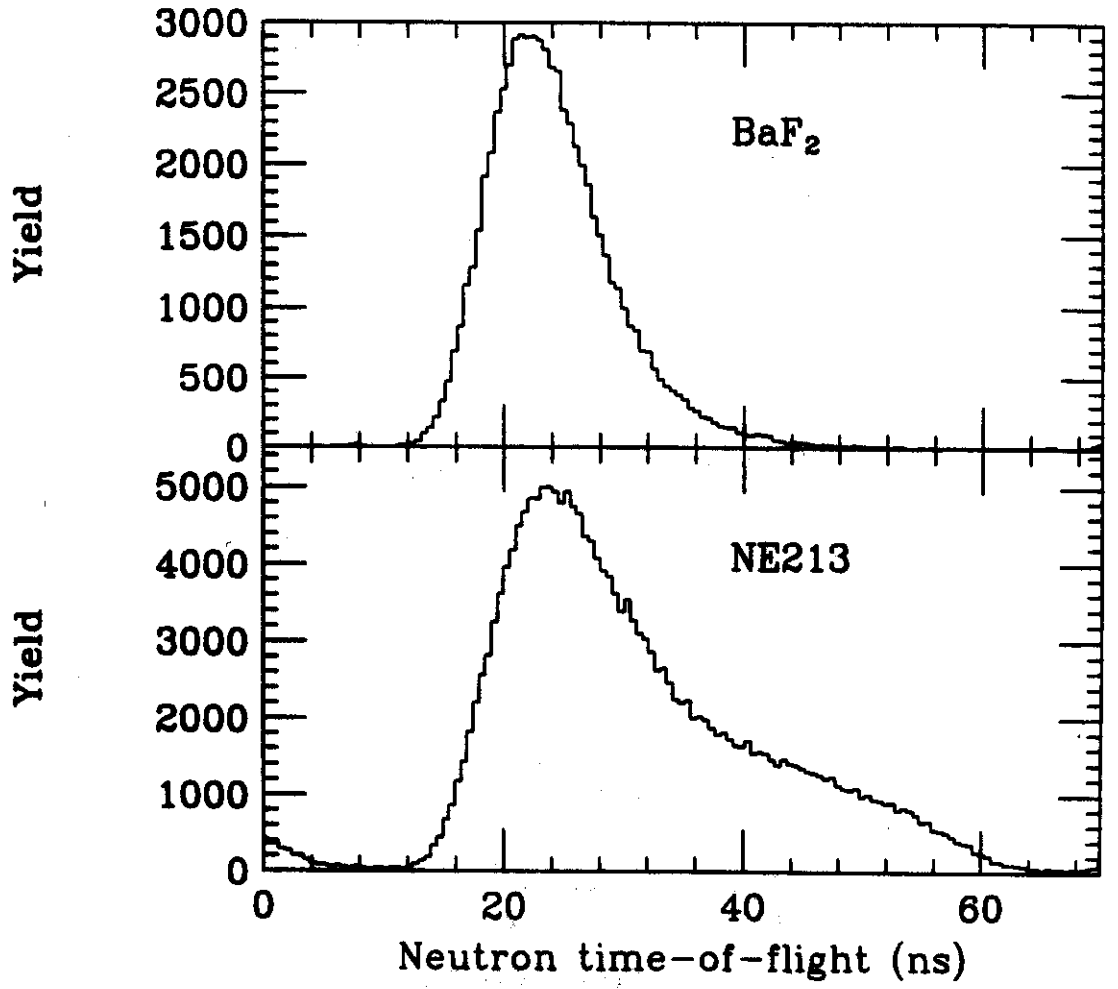
3000
2500
2000
1500
1000
500
0
Yield
BaF2
5000
4000
3000
2000
1000
0
Yield
NE213
0
20
40
60
Neutron time-of-flight (ns)

Figure 2

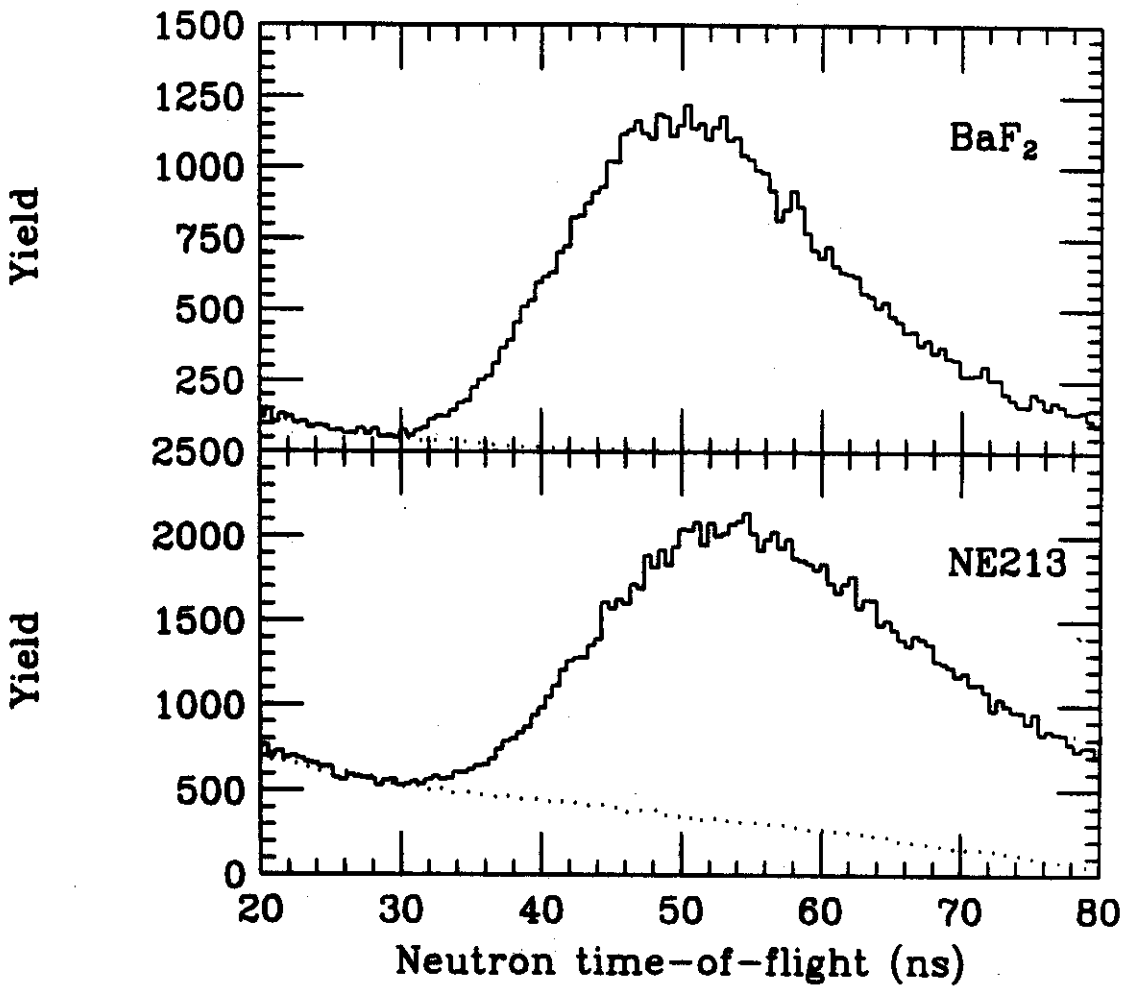
Yield
1500
1250
1000
750
500
250
0
BaF_2
Yield
2500
2000
1500
1000
500
0
NE213
20
30
40
50
60
70
80
Neutron time-of-flight (ns)

Figure 3

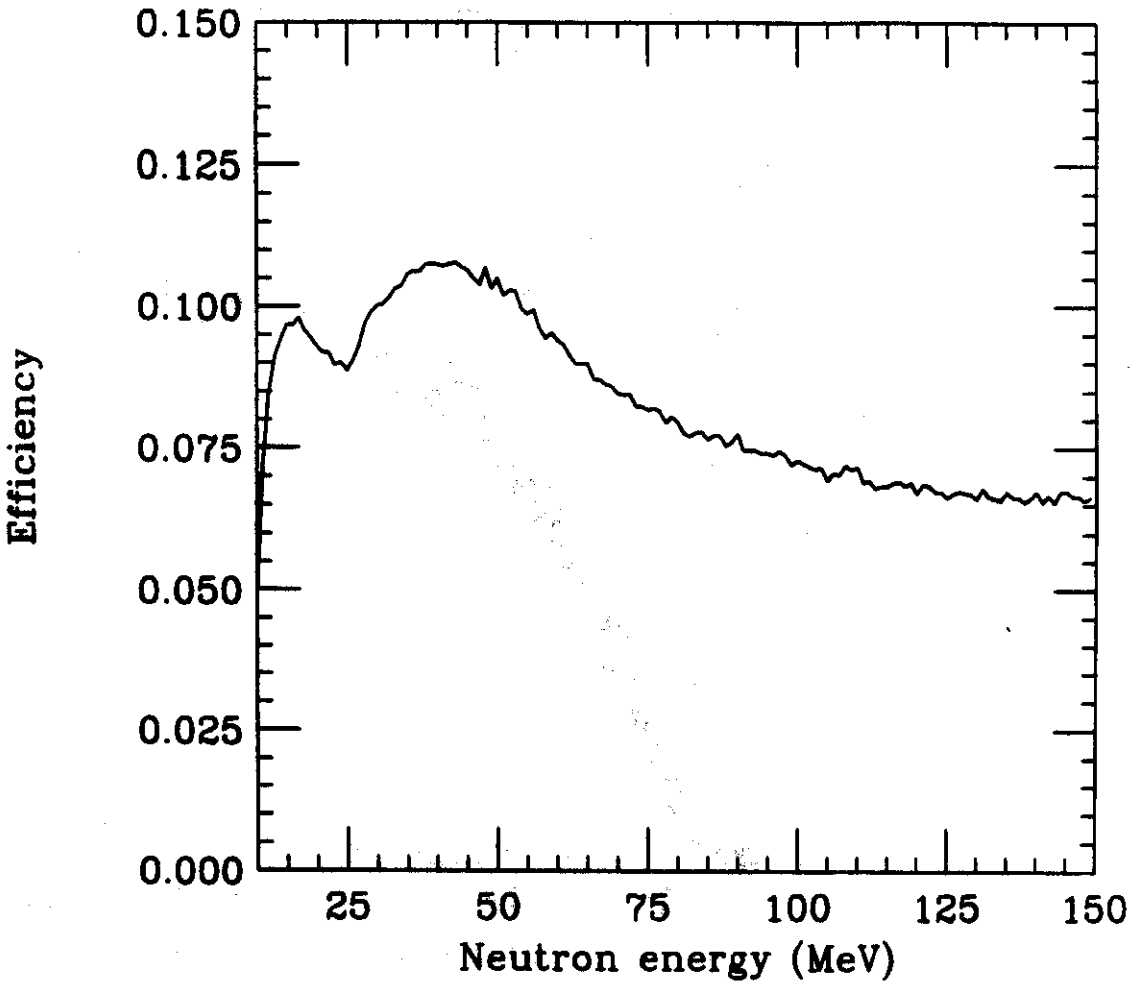
0.150
0.125
0.100
0.075
0.050
0.025
0.000
Efficiency
25
50
75
100
125
150
Neutron energy (MeV)

Figure 4

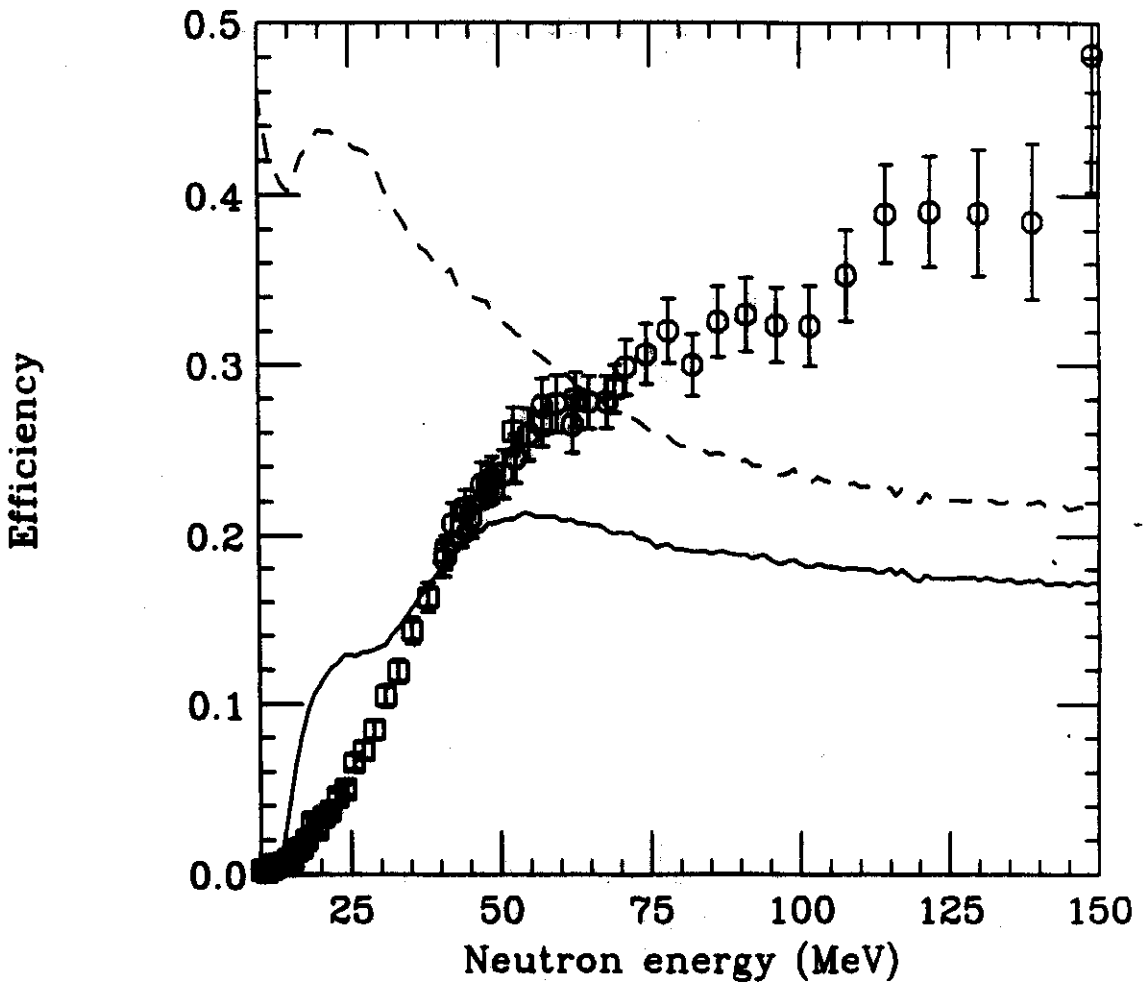
0.5
0.4
0.3
0.2
0.1
0.0
Efficiency
25
50
75
100
125
150
Neutron energy (MeV)

Figure 5

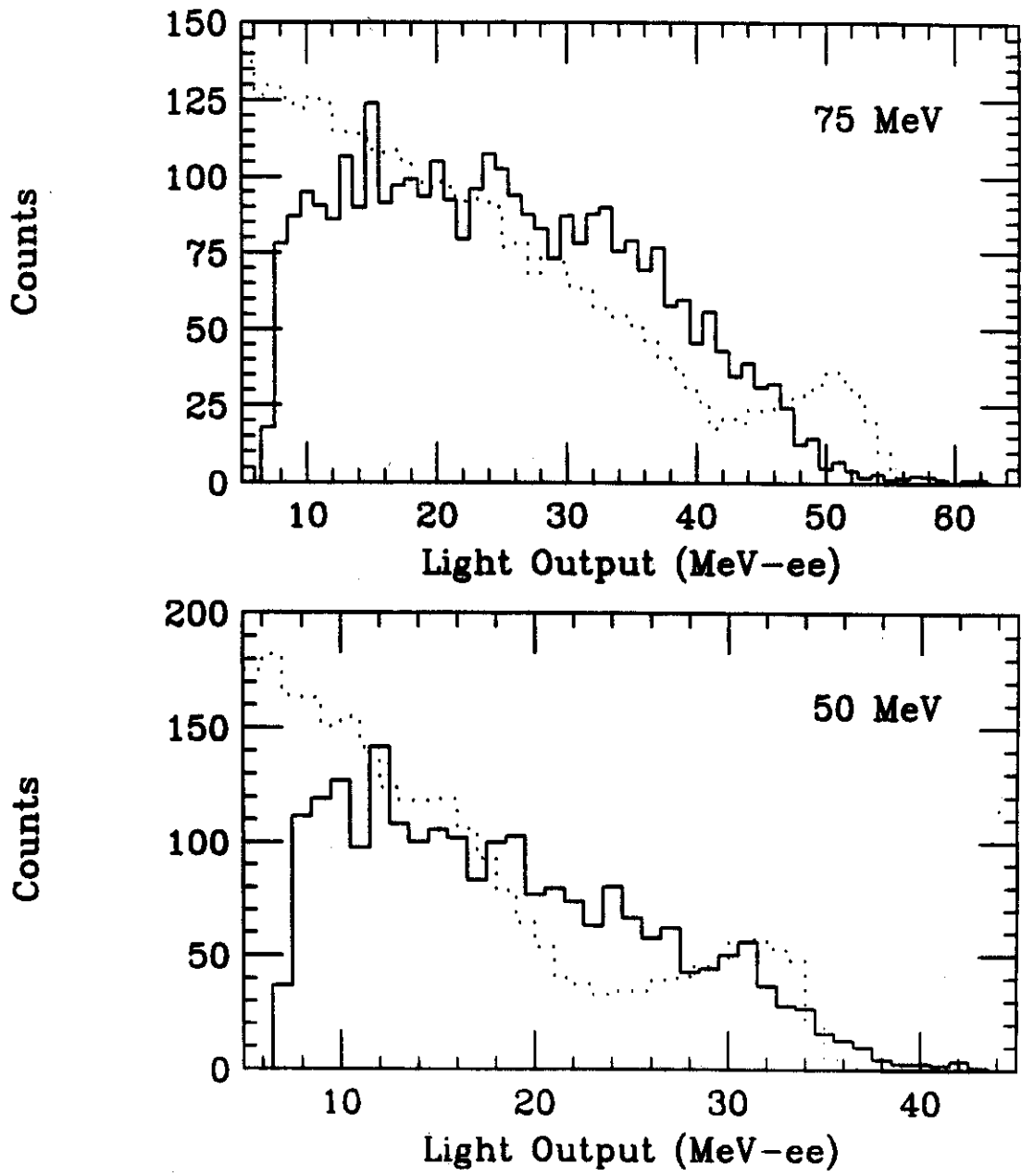
Counts
150
125
100
75
50
25
0
75 MeV
10
20
30
40
50
60
Light Output (MeV-ee)
Counts
200
150
100
50
0
50 MeV
10
20
30
40
Light Output (MeV-ee)